I&EC research
Industrial & Engineering Chemistry Research

Article

pubs.acs.org/IECR

Dip Coating of Fibers in the Visco-inertial Regime: Numerical Analysis

Diego M. Campana,[†,‡] Sebastián Ubal,[†,‡] María D. Giavedoni,*[,†] and Fernando A. Saita[†]

[†]INTEC (UNL−Conicet), Güemes 3450, 3000 Santa Fe, Argentina

[‡]Facultad de Ingeniería (UNER), C.C. 47, Suc. 3, 3100 Paraná, Argentina

ABSTRACT: The dip coating of a fiber of small radius is studied via a finite element solution of the Navier−Stokes equations. The coating speed is selected within the range corresponding to the visco-capillary and visco-inertial regimes. Predictions obtained within the range of the visco-capillary regime are in very good agreement with the Landau−Levich law and with published experiments, whereas those obtained within the visco-inertial regime—that is, at coating speeds typical of industrial applications—match published experimental data.

1. INTRODUCTION

The deposit of liquids on a solid is a common operation in everyday life as well as in the industry. In particular, a fiber coating is a usual process in the textile industry to give cohesion to multiple filaments, wash fibers, or provide them with specific properties. The process consists in withdrawing the fiber from a liquid bath in order to coat it with a film of small and uniform thickness. Coating speeds are usually between 5 to 30 m/s.

The first analysis of a dip coating process was carried out by Landau and Levich (1942)[1] and Deryagin (1943),[2] who studied the case of a plate when it is vertically pulled out of a liquid at very low velocities. They presented an expression, known as the Landau−Levich−Deryagin law (LLD for short), for the film thickness as a function of the capillary number. According to this theory, the thickness of the film results from the competition of viscous and capillary forces alone, a phenomenon that occurs only at very low coating speeds, when the film deposited is thin enough to neglect gravity effects. Thus the LLD law is rather restricted, and a considerable amount of work has been published thereafter to extend its validity by incorporating the effects of gravity, inertia forces, Marangoni stresses, etc.

De Ryck and Quéré (1996)[3] determined the thickness of the film formed when a cylindrical fiber is horizontally pulled out of the liquid contained inside a tube of 4 mm diameter. In their experiments, the withdrawal velocities ranged from 150 μm/s to 180 cm/s, the fiber radius was equal to either 63.5 or 12.5 μm, and the coating liquids were water and five silicon oils with viscosity equal to or greater than 19 cP. The results show that when the coating liquid is a silicone oil of high viscosity (i.e., when gravity and inertia forces are negligible), measured film thicknesses are in very good agreement with the correction proposed by White and Tallmadge[4] to extend the validity of the LLD law to larger capillary numbers. However, a completely different behavior is found with a low viscosity liquid, namely water, and coating speeds within the range 30−180 cm/s, that is, under conditions in which inertia forces are not always negligible. In this case, the film thickness only matches the LLD law if the capillary number is smaller than a given value, $Ca^* \approx 0.01$, above which the thickness of the entrained film sharply increases. By means of dimensional analysis, de Ryck and Quéré explain the reasons why inertia affects the film thickness, and they conclude, in agreement with the experiments, that the divergence between the experiments and the LLD predictions starts for values of the Webber number (i.e., the ratio between inertia and capillary forces) close to 1. The flow regime that sets in when this divergence occurs is called the visco-inertial regime. If the coating velocity is further increased, a third regime appears (the boundary-layer regime), in which the film thickness is limited by the geometry of the reservoir and no longer depends on surface tension.

More recently, Rebouillat et al.[5] presented experiments with a small fiber pulled out of a water bath. Their main objective was to quantify the effects of gravity on the film thickness in the visco-inertial regime. To that end, the tube was replaced by a "pocket bath" (see Figure 6 of reference 14), a device that allowed withdrawing the fiber at different angles of inclination. Also, the storage capacity of the reservoir was large, so that the impregnation of the fiber was not limited by a lack of liquid or influenced by the walls as it is likely to occur when the liquid bath is a drop trapped in a tube. They used a gravimetric method and a technique based on image analysis to determine the film thickness. Their results corroborate that gravity may be neglected when fibers are thin enough (less than 200 μm in diameter). Also, when the coating fluid is water and the radius of the fiber is 27 μm, their experiments confirm that the film thickness follows the LLD law for capillary numbers smaller than 0.008, and from this point on it sharply increases with the coating speed. However, they do not observe a thickness decrease at higher velocities as reported in reference 3 and they ascribe the discrepancy to the small size of the container used in that work. The analysis of the images captured show the evolution of the free surface shape as a function of the coating speed. These images prove the formation of drops in the meniscus region in the visco-inertial regime.

Received: March 7, 2013
Revised: August 2, 2013
Accepted: August 9, 2013
Published: August 9, 2013

dx.doi.org/10.1021/ie400751c | *Ind. Eng. Chem. Res.* 2013, 52, 12646−12653

Numerical solutions of the full hydrodynamic problem, including inertial effects,[6] soluble surfactants[7,8] and insoluble surfactants[9] have been obtained for planar substrates. However, it appears that —to the authors' best knowledge—no attempt has been made to numerically study the case of fiber coating at large velocities, that is, when the role of inertia cannot be neglected. Thus, the main goal of this work is to predict the film thickness formed on a cylindrical fiber pulled out of a liquid by numerically solving the Navier−Stokes equations; in particular, we are interested in comparing our predictions in the visco-inertial regime with some of the experiments already described.

The paper is organized as follows. In the next section we present the mathematical formulation of the problem. In section 3, we outline the numerical technique employed to solve the equations. In section 4, we discuss the computed predictions of the film thickness and compare them with published experiments. Finally, in section 5 we make some final remarks and delineate future work.

2. MATHEMATICAL FORMULATION

A small cylindrical fiber of radius b is vertically pulled out of a large liquid bath at constant speed U. The liquid is Newtonian with viscosity μ and density ρ. The air above it is considered inviscid and its pressure is arbitrarily set equal to zero. The fiber contacts the liquid at a distance H below the free surface; the coating fluid is a pure liquid and the temperature of the system is uniform; thus the gas−liquid surface tension, σ, is constant. Therefore, this process (see sketch in Figure 1) is governed by the Navier−Stokes and continuity equations that in dimensionless form read,

$$\nabla\cdot\mathbf{v} = 0 \tag{1}$$

$$Re\left(\frac{\partial \mathbf{v}}{\partial t} + \mathbf{v}\cdot\nabla\mathbf{v}\right) = -\frac{1}{Ca}\nabla p + \nabla^2\mathbf{v} - \frac{Bo}{Ca}\mathbf{e}_z \tag{2}$$

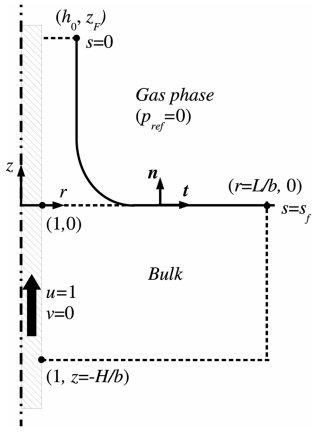

Figure 1. Sketch of the flow domain and coordinate system adopted.

The characteristic scales used are U for velocities, b for lengths, b/U for time, σ/b for pressure, and $\mu U/b$ for the components of the stress tensor; in the above expressions, $Re = \rho bU/\mu$ is the Reynolds number, $Ca = \mu U/\sigma$ is the capillary number, and $Bo = \rho g b^2/\sigma$ is the Bond number that measures the ratio between gravity and capillary forces. The Bond number can also be written as $Bo = (b/l_C)^2$, where l_C is the capillary length which, for most of the liquids is of order of 1 mm. Thus, if b is not larger than 100 μm, $Bo \leq 0.01$, and gravity effects can be safely neglected.

The boundary conditions imposed are as follows. On the surface of the fiber the nonslip condition is enforced; that is,

$$u = 1, \quad v = 0, \quad -H^* \leq z \leq z_F, \quad r = 1 \tag{3}$$

where u and v are the dimensionless components of the velocity in the z and r directions, respectively, and $H^* = H/b$.

At the bottom boundary, the flow does not change along the z coordinate. Also, we substitute the pressure by its hydrostatic value in the normal component of the stress; thus, the following expression is used

$$\mathbf{T}\cdot(-\mathbf{e}_z) = \frac{BoH^*}{Ca}\mathbf{e}_z - \frac{\partial u}{\partial r}\mathbf{e}_r, \quad z = -H^*, \ 1 < r \leq L^* \tag{4}$$

where $\mathbf{T}$ stands for the stress tensor, and $L^* = L/b$.

At the lateral boundary of the domain which is located at a distance L^*, far away from the fiber, the flow is in the radial direction only. In addition, we assume that the pressure is mainly hydrostatic; therefore, the traction vector results as follows

$$\mathbf{T}\cdot\mathbf{e}_r = \left(\frac{Boz}{Ca} + 2\frac{\partial v}{\partial r}\right)\mathbf{e}_r + \frac{\partial v}{\partial z}\mathbf{e}_z, \quad r = L^*, \ 0 \leq z \leq -H^* \tag{5}$$

At the film exit boundary, we assume that the flow is unidirectional and does not change in the axial direction; thus, the traction vector is

$$\mathbf{T}\cdot\mathbf{e}_z = -\frac{p}{Ca}\mathbf{e}_z + \frac{\partial u}{\partial r}\mathbf{e}_r, \quad z = z_F, \ 1 \leq r \leq h_0 + 1 \tag{6}$$

To establish the boundary conditions at the free surface, we presume that the interface is a material surface; therefore, the kinematic condition applies

$$\mathbf{v}\cdot\mathbf{n} = \dot{\mathbf{x}}_{FS}\cdot\mathbf{n} \tag{7}$$

In the above expression, $\dot{\mathbf{x}}_{FS}$ is the velocity of the nodes at the free surface and $\mathbf{n}$ is the outwardly directed unit vector normal to the interface.

The free surface is Newtonian and inviscid; hence, the dimensional surface stress tensor, $\mathbf{T}^{(S)}$, is $\mathbf{T}^{(S)} = \sigma(\mathbf{I} - \mathbf{nn})$, $\mathbf{I}$ being the identity tensor. Since the system is free of surfactant, surface tension is constant; thus the dimensionless interfacial balance of stresses results

$$\mathbf{n}\cdot\mathbf{T} = \frac{1}{Ca}\left[\frac{d\mathbf{t}}{ds} - \frac{(\mathbf{e}_r\cdot\mathbf{n})\mathbf{n}}{r_S}\right] \tag{8}$$

where r_S is the local free surface radius, and $\mathbf{t}$ is the unit vector tangent to the free surface pointing toward increasing values of the arc-length s (see Figure 1).

Finally, we specify the tangent vector at both ends of the interface; that is, $\mathbf{t} = \mathbf{e}_r$ at $s = s_f$, and $\mathbf{t} = -\mathbf{e}_z$ at $s = 0$.

In the next section we summarize the numerical technique employed to solve the system of governing equations and boundary conditions eq 1−8.

3. NUMERICAL TECHNIQUE

The system of governing equations and their boundary conditions is discretized using the Galerkin/Finite Element

dx.doi.org/10.1021/ie400751c | Ind. Eng. Chem. Res. 2013, 52, 12646−12653

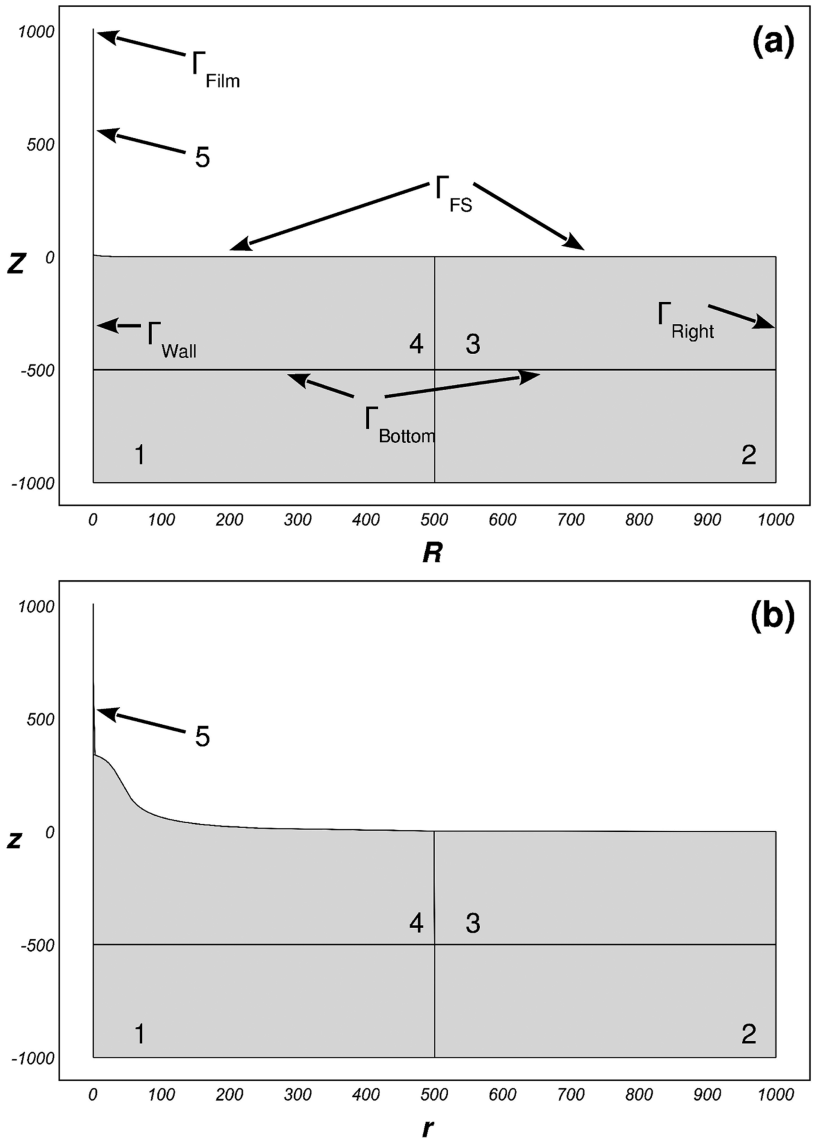

Figure 2. (a) Definition of the reference domain and its associate boundaries, and (b) physical domain where the flow equations are formulated.

method, along with an ALE (*Arbitrary Lagrangian Eulerian*) technique to take into account the changes in the flow domain as the iteration proceeds. The residuals are built following the procedure described in previous works.[10−12]

Since there is a gas/liquid interface with unknown location and shape, we find it expedient to compute first an approximate steady-state solution for a particular set of the parameters (*Re*, *Ca*, and *Bo*) by solving the transient problem, and then to obtain the exact solution by solving the steady-state problem using the approximate solution as the initial guess. From this point on, we trace the space of the parameters with a zero-order continuation procedure.

When the deformation of the flow domain is large, it is advantageous to employ an unstructured mesh of triangular elements. The ALE algorithm implemented is briefly discussed in what follows.

The starting point is a regular domain (the reference domain) whose shape is invariant in the reference frame with coordinates (*R*, *Z*). We also consider an irregularly shaped domain in the physical space with coordinates (*r*, *z*). Both domains are related by the mapping: $r = r(R, Z, t)$, $z = z(R, Z, t)$.

The mapping is found by solving a partial differential equation with appropriate boundary conditions for the coordinates located in the regions where the mesh deforms; in the Winslow's algorithm[13] implemented in this work, the PDE used is

$$\nabla^2 \mathbf{R} = 0 \Rightarrow \begin{cases} r \text{ component: } \dfrac{\partial^2 R}{\partial r^2} + \dfrac{\partial^2 R}{\partial z^2} = 0 \\ z \text{ component: } \dfrac{\partial^2 Z}{\partial r^2} + \dfrac{\partial^2 Z}{\partial z^2} = 0 \end{cases} \tag{9}$$

A drawback of ALE methods is that movement of the nodes can be very large, giving rise to distorted mesh elements with poor numerical quality and even inverted overlapped elements. Under these circumstances the numerical algorithm does not converge to a solution and the zero-order continuation process stops. If this is the case we proceed as follows

The simulation is stopped.

The last converged spatial configuration (i.e., the last deformed domain) is detected.

This configuration is saved as the new reference configuration.

A remeshing of the new reference configuration is performed.

Once a converged stationary solution is obtained, the continuation process is restarted.

The computational domain is conveniently divided in the regions shown in Figure 2. In regions 1 and 2, far away from the free surface, the mesh is fixed and the Navier−Stokes and continuity equations have to be solved. In all the other zones the mesh is adapted; therefore, in addition to Navier−Stokes and continuity, eq 9 has to be solved there to obtain the spatial coordinates of the nodes.

The boundary conditions applied are as follows:

Because the free surface is a material boundary, the kinematic condition (7) is imposed on Γ_S; thus, the interfacial nodes move with the normal component of the fluid velocity.

On Γ_{Bottom} the nodes are fixed.

On Γ_{Right} and Γ_{Wall} the nodes are restricted to move in the z direction.

On Γ_{Film} ($z = z_f$, $1 < r < h_0$) the nodes are restricted to move in the r direction.

We solve the equations described in section 2 with COMSOL Multiphysics (COMSOL Inc., 1998−2001). The domain is tessellated using an unstructured mesh of triangles; radial and axial velocities as well as coordinates are interpolated by piecewise quadratic Lagrange polynomials, whereas the pressure is interpolated by linear ones.

COMSOL Multiphysics handles the kinematic eq 7 by means of the Lagrange's multipliers technique. The resulting set of nonlinear algebraic equations is simultaneously solved using a Newton's loop. The convergence criterion adopted is that the norm of the difference between two consecutive approximations is equal to or smaller than 10^{-5}. When a transient simulation is carried out, the time derivatives are approximated using finite differences and a second order adaptive time step algorithm is used. Moreover, since the expressions of the governing equations are given on fixed spatial coordinates, node velocities must be taken into account to correctly evaluate the time derivatives.

We next describe the main features of the simulations. To determine an appropriate size for the flow domain, the different length scales between the film and the bulk must be considered. Numerical tests carried out show that within the range of the parameters studied in this work, the order of the film thickness varies between $10^{-2}b$ and b, and that the extension of the dynamic meniscus along the radial and axial directions varies between $10b$ and $1000b$. These dimensions determine the lengths H^*, L^* and z_f (see Figure 1) that must be chosen to fulfill boundary conditions eq 4−6. We find adequate to fix $H^* = L^* = z_f = 1000$. Since lengths are measured in units of the radius of the fiber—which in this work is set equal to either 12.5 or 63.5 μm—the corresponding dimensional quantities are equal either to 1.25 cm or 6.35 cm.

Once the size of the computational domain is established, it is split in various subdomains (see Figure 2) according to the characteristics presented by the flow. The finite element mesh is more refined along and in the vicinity of the free surface, especially in the meniscus and film regions, and the size of the elements gradually increases as one moves away from the free surface. In the dynamic meniscus region as well as in the area where the film region begins, the size of the elements is 4−5 times smaller than the film thickness. The characteristics of the flow domain strongly depend on the magnitude of inertia forces; the number of elements of the finite element meshes used to compute the solutions presented in this work ranges from 250 000 to 300 000, which results in 2 100 000 and 2 500 000 degrees of freedom, respectively.

In the simulations carried out with "iso 5" oil (see next section), the domain configuration and the mesh adopted for $Ca = 0.01$ were satisfactorily adapted by the ALE method and Winslow algorithm when $Ca \leq 0.135$. At this value of the capillary number, a new reference domain was defined and remeshed. This domain allowed us to compute solutions up to the largest value of Ca considered in this paper.

When water is the coating fluid (see next section), the size of the domain and the mesh adopted for $Ca = 0.001$ are appropriate up to $Ca = 0.015$. At this value of the capillary number, we adopted a new reference domain which was conveniently remeshed and allowed us to compute solutions for values of $Ca \leq 0.0202$.

The largest values of Ca for which we were able to compute solutions for the two liquids considered in this work are near the region where the visco-inertial regime merges into the boundary layer regime. The lack of convergence of the numerical method might be due to either this fact or to the nonexistence of steady state solutions as it is discussed in the next section.

It is worthy to mention that the remeshing process produces variations in the film thickness not larger than 0.5%; also, changes in the interfacial shape are negligible.

Finally, to validate the computer code, we solved the problem for $Re = 0$ and within the range of Ca where the Landau−Levich law accurately predicts the film thickness. Results are presented in the next section.

4. RESULTS AND DISCUSSION

4.1. The Evolution of the Film Thickness. When the fiber is small (i.e., its radius is much smaller than the capillary length, l_C) and the withdrawal velocity is low, the effects of gravity and inertia are both negligible and the process depends on the competition between viscous and capillary forces. In this

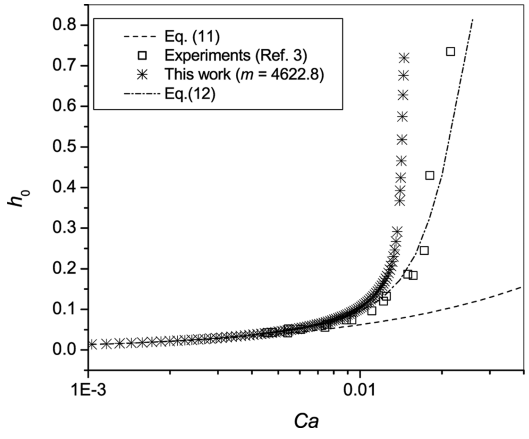

Figure 3. Dimensionless film thickness entrained by a fiber of radius b = 63.5 μm withdrawn from pure water as a function of the capillary number.

dx.doi.org/10.1021/ie400751c | Ind. Eng. Chem. Res. 2013, 52, 12646−12653

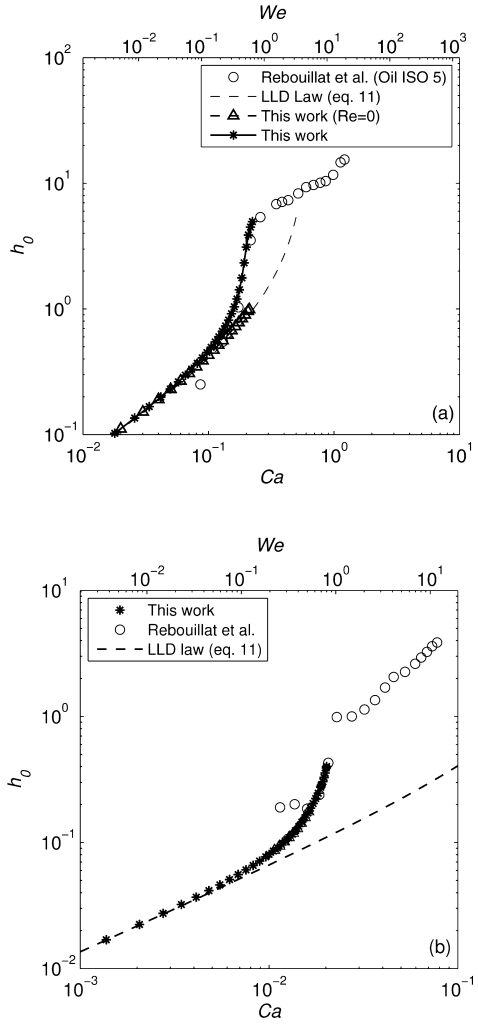

Figure 4. Film thickness predictions as a function of the capillary number for (a) m equal to 0 and 12.92 (Oil ISO 5), and (b) m equal to 1962.08 (water).

case the film thickness can be accurately estimated using the LLD expression; that is,

$$h_0 = 1.34Ca^{2/3} \tag{10}$$

When the capillary number approaches 1 and the liquid viscosity is large enough so that inertia forces are still negligible, the film thickness can be of the same order as the radius of the fiber; consequently, the assumption that the thickness of the deposited film is much smaller than the radius of the fiber is not accomplished and eq 10 is not longer valid. White and Tallmadge[4] proposed a simple correction that consists in replacing the dimensionless radius of the fiber (that is, 1) by the dimensionless radius of the free surface (i.e., $1 + h_0$) in eq 10; thus, the resulting expression for the film thickness is

$$h_0 = \frac{1.34Ca^{2/3}}{1 - 1.34Ca^{2/3}} \tag{11}$$

As we have already mentioned in the Introduction, the main goal of the present work is to numerically analyze the impregnation of a fiber in the visco-inertial regime. To that end we made computations in the range of parameters corresponding to the experiments performed by de Ryck & Quéré[3] and Rebouillat et al;[5] therefore, the liquids considered were water ($\mu = 1.0 \times 10^{-3}$ Pa s, $\rho = 998.21$ kg/m^3, and $\sigma = 7.28 \times 10^{-2}$ N/m) and "iso 5" oil ($\mu = 6.5 \times 10^{-3}$ Pa s, $\rho = 822$ kg/m^3, and $\sigma = 2.46 \times 10^{-2}$ N/m), the radius of the fiber was set equal to 63.5 μm, the value of the nickel wire used by de Ryck and Quéré, and to 27 μm, which corresponds to the nylon filament used by Rebouillat et al. In our numerical experiments the coating speed was varied within the experimental range. Since both the Reynolds and the capillary number simultaneously change with U, the ratio $m = Re/Ca = \rho\sigma b/\mu^2$ (usually known as the Laplace number) was kept constant in the simulations.

Figure 3 illustrates the thickness of the film formed on a 63.5 μm fiber as a function of the capillary number when the coating liquid is water. Reported values correspond to measurements by de Ryck & Quéré, to numerical solutions of eqs 1 to 8, and to the evaluation of the following expression:

$$h_0 = \frac{1.34(1 + h_0)Ca^{2/3}}{1 - W\beta(h_0)} \tag{12}$$

The above formula is an approximate solution to the evolution equation of the film thickness published by Koulago et al. (1995);[15] it was obtained by Quéré and de Ryck (1998)[16] assuming that the thickness of the free surface is limited by the radius of the tube used as reservoir. In eq 12, $W = \rho U^2 b(1 + h_0)/\sigma$ is a Weber number (i.e., the ratio between the dynamic and the capillary pressures), and β is a logarithmic function of the ratio between the film thickness and the tube radius. Predictions of eq 11 are also depicted in the figure.

It is easy to see that the threshold $Ca = Ca^*$, i.e. the capillary value above which the film sharply thickens as the coating speed further increases is well predicted by both the numerical solution and eq 12. In their paper, de Ryck & Quéré[3] argued that the transition from the visco-capillary to the visco-inertial regime takes place when inertia and surface forces are comparable in magnitude, that is, when the Weber number defined as $We = \rho U^2 b/\sigma$ is approximately on the order of 1. A simple calculation shows that for the fiber and liquid considered, the velocity at the threshold is $U^* \approx 1$ m/s, and thus $Ca^* \approx 0.014$ which is a value close to that measured or predicted ($Ca^* \approx 0.01$).

The curves illustrated in Figure 3 also show good agreement between the film thickness calculated with eq 12 and the experimental data, within the whole range of Ca. Considering that eq 12 is an approximate solution of a 1D model, the match is indeed surprising. On the other hand, the numerical predictions depicted in Figure 3 were obtained with the mathematical model already described in section 2. That model accounts for gravity effects and represents the withdrawal of the fiber from a large liquid reservoir; instead in the experiments the fiber is pulled out from a horizontal tube of small radius (2 mm). Our numerical predictions fit the experiments only if the Ccapillary number is smaller than approximately 0.01; for larger values they are substantially thicker than the experimental ones. Obviously, gravity cannot be responsible for the difference between experiments and calculations because it tends to limit the thickness of the film; moreover, in the region where experiments and the LLD law diverge, both the Bond number ($Bo = b^2/l_C^2$) and the reciprocal of the Froude number ($Fr = U^2/2gb$) are much smaller than one indicating that gravity has no influence at all. Hence we might assume that at large coating speeds the tube wall limits the amount of liquid entrained by the fiber; actually, for the case shown in Figure 3, we will see in

dx.doi.org/10.1021/ie400751c | Ind. Eng. Chem. Res. 2013, 52, 12646−12653

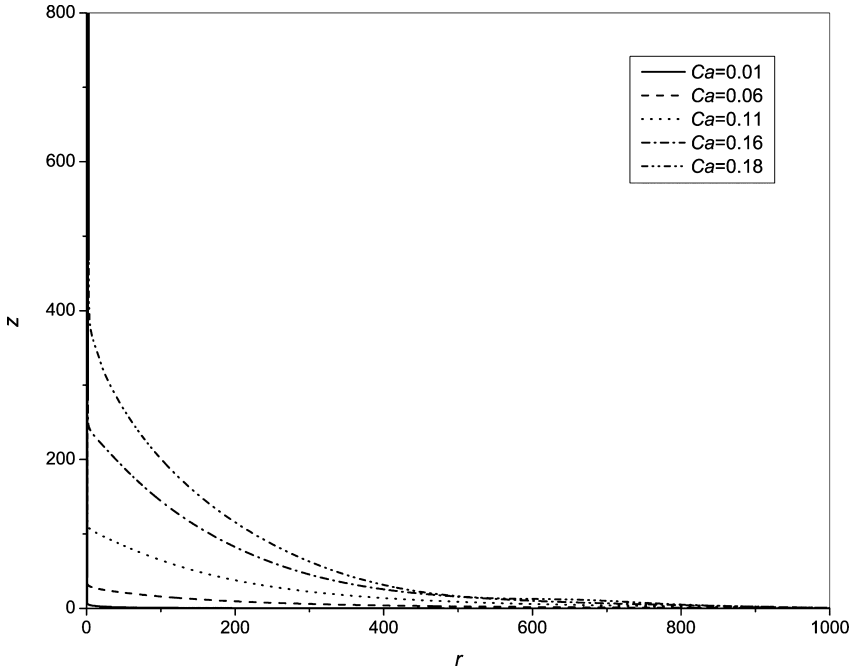

Figure 5. Free surface shapes for selected values of *Ca*. The fiber (b = 27 μm) is withdrawn from a large reservoir of iso 5 oil (m = 12.92).

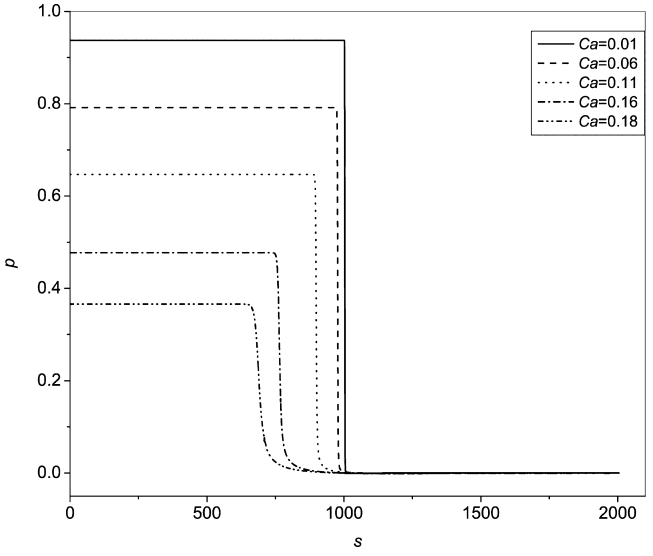

Figure 6. Pressure distribution along the free surface for the cases shown in Figure 5.

the next section that the height and the radial extent of the meniscus increase with the coating speed and consequently it might interact with the walls of a small reservoir such as the one used in the experiments reported by de Ryck and Quéré at capillary values as low as 0.01 or even lower. Nonetheless, to shed some light into the hypothesis that the tube wall restricts liquid flow, we carried out numerical computations under the conditions of the experiments implemented by Rebouillat et al.[5]

In Figure 4, numerical predictions of the film thickness and measurements reported by Rebouillat et al. are plotted as a function of *Ca* when the coating liquid is either water or the iso 5 oil; also, numerical solutions for m = 0 and values resulting from expression (11) are drawn for reference. The experiments were carried out with a nylon fiber of b = 27 μm.

When inertia forces are neglected, (i.e., m = 0), the results of eq 11 agree with our numerical predictions until $Ca \approx 0.2$ although slight deviations are noticed for $Ca > 0.1$. If inertia forces are considered ($Re = mCa$), a similar behavior to that reported in Figure 3 occurs, the main difference being that now the predictions are in good agreement with the experiments even above the threshold *Ca* at which the film thickness diverges from LLD law. This is particularly noticeable in the case of the oil, where we were able to compute solutions up to the beginning of what appears to be a transition region between visco-inertial and boundary layer regimes (cf. de Ryck and Quéré, 1996).

The excellent agreement between the pocket bath experiments and the numerical predictions, as well as the trend followed by the results illustrated in Figures 3 and 4, support the hypothesis that the tube wall opposes the thickening of the film in the visco-inertial regime.

For a given fiber radius (27 μm for the results shown in Figure 4), the threshold capillary number (Ca^*) at which the departure from the LLD law occurs depends on the fluid, as expected. It is approximately equal to 0.01 for water (m = 1962.08) and to 0.1 for the iso 5 oil (m = 12.92). As we have mentioned above, the visco-inertial regime takes place when the Webber number is of order one. Simple calculations show that U^* is 1.05 m/s for the oil and 1.64 m/s for water, and therefore Ca^* will be roughly larger than 0.02 and 0.27 for water and oil, respectively; these values are fairly close to those reported in Figure 4.

We were not able to compute solutions with any of the liquids near the transition between the visco-inertial and the boundary layer regimes; in fact, the largest coating speed numerically explored was 167.4 cm/s (Ca = 0.023) for water and 84.7 cm/s (Ca = 0.224) for the oil. One possible reason for the lack of convergence could be an inappropriate size of the computational domain or an unsuitable mesh to follow the modifications undergone by the flow domain in that region. To check these hypotheses we should have to enlarge the domain

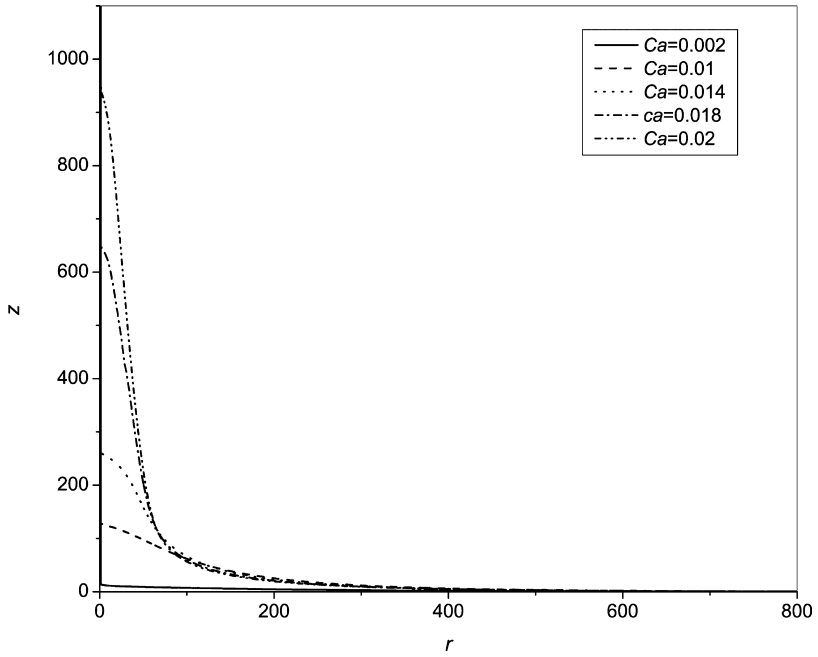

Figure 7. Free surface shapes for selected values of *Ca*. The fiber (b = 27 μm) is withdrawn from a large reservoir of water (m = 1962.08).

and/or refine the mesh, but unfortunately that is not possible with our present computational resources. Another explanation can be related to the following experimental finding that suggests a time-periodic behavior of the system above a given capillary number: Rebouillat et al.[5] observed a cyclic evolution of the meniscus shape (see Figure 8 of ref 5) that involves the formation and drag of a water drop when $Ca \approx 0.02$ suggesting that above a certain (m-dependent) capillary number steady state solutions do not exist or are not stable. The reason why the transition from steady state to a cyclic evolution is detected at a capillary number smaller than the maximum value we attained (Ca = 0.023), might be due to perturbations induced by experimental features —such as a small amplitude vibration of the fiber. In addition, we performed several computations of the transient flow problem in the vicinity of Ca = 0.02; all of them led to the corresponding steady state solution hinting that larger perturbations than those brought forth during a transient computation are required to destabilize the system.

4.2. The Evolution of the Meniscus Shape. For capillary numbers well below Ca^* the film thickness results from the competition between viscous and capillary forces and the film thickness is well predicted by LLD law. Above the threshold Ca^* the strength of inertia becomes noticeable and reinforces the action of viscous forces: they both weaken the capillary suction effect in the dynamic meniscus, which tends to limit the fluid entrained by the fiber; therefore, a larger amount of liquid is dragged by the solid as the coating speed increases. The shapes illustrated in Figure 5 for the iso 5 oil (m = 12.92) show that the size of the meniscus strongly depends on the coating speed. In fact, both its height and its radial extent increase with U; for Ca = 0.18, it is almost as wide as the computational domain (2.7 cm) and the film is formed at a distance larger than 430b above z = 0.

Figure 6 illustrates the pressure as a function of the arc length for the same five cases portrayed in Figure 5; the arc length is measured from the film toward the liquid bath. As expected, the pressure is equal to zero far away from the fiber and it becomes equal to the capillary pressure $[1/(1 + h_0)]$ in the film. Since the film thickens as the coating speed increases, the capillary pressure diminishes: it is almost three times smaller for Ca = 0.18 than for Ca = 0.01. Also, the curves depicted in the figure show that the pressure jump decreases as the coating speed is augmented while the region where the pressure transition occurs moves toward the end of the computational domain ($z = z_p$, s = 0) and becomes larger.

The effects of inertia forces are more evident in Figure 7, where the meniscus of water (m = 1962.08) is depicted for selected values of the capillary number. The meniscus is now similar to a cylinder whose height increases with the coating speed, being as large as 900b when Ca = 0.02 (i.e., $U \approx$ 1.45 m/s). It is interesting to note the similarity between the configurations shown in this figure and some of the images reported by Rebouillat et al. (see Figure 8 of ref 5) corresponding to their experiments with water. However, we have to remark once again that those images exhibit a cyclic change of the meniscus at $Ca \approx 0.02$: first the meniscus adopts a cylindrical shape similar to those illustrated in Figure 7, and then drops are formed and dragged by the fiber.

At low speeds, Figure 7 shows another interesting result: r = 100 represents a distance of 2.7 mm from the fiber wall; as the figure shows, this location begins to be reached by the interfacial meniscus for capillary values even smaller than 0.01. This means that a wall located at such a distance from the fiber must have influence on the amount of liquid being drawn. Apparently, this is what happens in the experiments performed by de Ryck and Quéré,[3] in which they withdraw a fiber from the coating liquid contained in a tube of 2 mm radius. In Figure 3 we can see that our numerical predictions start to depart from their results when $Ca \approx 0.008$.

5. CONCLUSION

In this work we present numerical solutions of dip coating of thin fibers being withdrawn from liquid pools at least 3 orders of magnitude larger than the fiber radius. The model was validated by comparing its predictions with the LLD theory and it was used to reproduce already published experiments carried

out in the visco-inertial regime. In the region where the visco-inertial regime starts to prevail, our numerical predictions agree surprisingly well with the experiments performed by Rebouillat et al. (2002); however, they differ substantially from the experiments published by de Ryck and Quéré (1996), in which they used a tube of 4 mm diameter to contain the liquid to be coated. We give evidence that the discrepancies are due to the solid walls of the tube that restrain the liquid motion.

The experiments of Rebouillat et al. indicate that at a certain coating speed the visco-inertial regime appears to make a transition to another regime, a change that is evidenced by a change in the slope of the curve of film thickness versus *Ca*. Our computation fails to make that transition and the numerical code does not converge just at the end of the visco-inertial regime. The lack of convergence might be caused by an unsuitable mesh that cannot cope with the large modifications that the flow domain is suffering in that region, or it might be because the flow becomes transient at that point. This second possibility is supported by the cyclic evolutions of the meniscus shape that Rebouillat et al. observed shortly before the end of the vico-inertial regime. New analyses are being undertaken to shed light on the probable cause of the failure.

AUTHOR INFORMATION

Corresponding Author

*E-mail: madelia@santafe-conicet.gov.ar.

Notes

The authors declare no competing financial interest.

ACKNOWLEDGMENTS

We gratefully acknowledge ANPCyT, UNL, and CONICET for financially supporting this work.

REFERENCES

(1) Landau, L.; Levich, B. Dragging of a liquid by a moving plate. *Acta Physicochim. URRS* **1942**, *17*, 42.
(2) Deryagin, B. V. Thickness of liquid layer adhering to walls of vessels on their emptying and the theory of photo and motion picture film coating. *Acta Physicochim. USSR* **1943**, *39*, 13.
(3) De Ryck, A.; Quéré, D. Inertial coating of a fibre. *J. Fluid Mech.* **1996**, *311*, 219.
(4) White, D. A.; Tallmadge, A. A theory of withdrawal of cylinders from liquid baths. *AIChE J.* **1966**, *12*, 333.
(5) Rebouillat, S.; Steffenino, B.; Salvador, B. Hydrodynamics of high-speed fibre impregnation: The fluid layer formation from the meniscus region. *Chem. Eng. Sci.* **2002**, *57*, 3953.
(6) Jin, B.; Acrivos, A.; Münch, A. The drag-out problem in film coating. *Phys. Fluids* **2005**, *17*, 103603−1.
(7) Krechetnikov, R.; Homsy, G. M. Surfactant effects in the Landau−Levich problem. *J. Fluid Mech.* **2006**, *559*, 429.
(8) Campana, D. M.; Ubal, S.; Giavedoni, M. D.; Saita, F A. Numerical prediction of the film thickening due to surfactants in the Landau−Levich problem. *Phys. Fluids* **2010**, *22*, 032103−1.
(9) Campana, D. M.; Ubal, S.; Giavedoni, M. D.; Saita, F A. A deeper insight into the dip coating process in the presence of insoluble surfactants: A numerical analysis. *Phys. Fluids* **2011**, *23*, 052102−1.
(10) Giavedoni, M. D.; Saita, F. A. The axisymmetric and plane cases of a gas phase steadily displacing a Newtonian liquid −A simultaneous solution of the governing equations. *Phys. Fluids* **1997**, *9*, 2420.
(11) Campana, D.; Saita, F. A. Numerical analysis of the Rayleigh instability in capillary tubes.−The influence of surfactant solubility. *Phys. Fluids* **2006**, *18*, 022104 1.
(12) Ubal, S.; Giavedoni, M. D.; Saita, F. A. A numerical analysis of the influence of the liquid depth on two dimensional Faraday waves. *Phys. Fluids* **2003**, *15*, 3099.
(13) Winslow, A.M.. Equipotential zoning of two-dimensional meshes. *Report UCRL-7312*; University of California, Lawrence Radiation Laboratory: Berkeley, CA, 1963.
(14) Rebouillat, S.; Steffino, B.; Letellier, B. Hydrodynamics of high speed fibre impregnation. *Chem. Eng. Sci.* **2000**, *55*, 15.
(15) Koulago, A.; Shkadov, V.; Quéré, D.; de Ryck, A. Film entrained by a fiber quickly drawn out of a liquid bath. *Phys. Fluids* **1995**, *7*, 1221.
(16) Quéré, D.; de Ryck, A. Les mouillage dynamique des fibres. *Ann. Phys. Fr.* **1998**, *23*, 1.